AUTHOR QUERY FORM

AIP Publishing	**Journal: J. Appl. Phys.** **Article Number: JAP24-AR-05591**	**Please provide your responses and any corrections by annotating this PDF and uploading it to AIP's eProof website as detailed in the Welcome email.**

Dear Author,

Below are the queries associated with your article; please answer all of these queries before sending the proof back to AIP.

Article checklist: In order to ensure greater accuracy, please check the following and make all necessary corrections before returning your proof.

1. Is the title of your article accurate and spelled correctly?
2. Please check affiliations including spelling, completeness, and correct linking to authors.
3. Did you remember to include acknowledgment of funding, if required, and is it accurate?

Location in article	Query / Remark: click on the Q link to navigate to the appropriate spot in the proof. There, insert your comments as a PDF annotation.
Q1	Please check that the author names are in the proper order and spelled correctly. Also, please ensure that each author's given and surnames have been correctly identified (given names are highlighted in red and surnames appear in blue).
Q2	Please reword the sentence beginning with "It originates that ..." so that your meaning will be clear to the reader.
Q3	Please reword the sentence beginning with "It origins that ..." so that your meaning will be clear to the reader.
Q4	The sentence beginning with "The biaxial strain is a repetition of a previous sentence beginning with "Additionally, the biaxial strain ...". Please check and indicate if any changes are required.
Q5	Please reword the sentence beginning with "It origins that ..." so that your meaning will be clear to the reader.
Q6	Please reword the text "It origins that..." so that your meaning will be clear to the reader.
Q7	Please reword the sentence beginning with "We find that ..." so that your meaning will be clear to the reader.
Q8	We were unable to locate a digital object identifier (doi) for Refs. 1, 7, 15, 24, and 64. Please verify and correct author names and journal details (journal title, volume number, page number, and year) as needed and provide the doi. If a doi is not available, no other information is needed from you. For additional information on doi's, please select this link: http//www.doi.org/.

	Please confirm ORCIDs are accurate. If you wish to add an ORCID for any author that does not have one, you may do so now. For more information on ORCID, see https://orcid.org/. Linhui Lv Fangyu Zhang Diancong Qi Zihao Xu–0009-0009-4499-8240 Weiyi Wang–0000-0001-6981-2611 Ya Su–0000-0001-9136-6726 Yanyan Jiang Zhaoyong Guan–0000-0002-6847-5809
	Please check and confirm the Funder(s) and Grant Reference Number(s) provided with your submission: Natural Science Foundation of China, 11904203 Fundamental Research Funds of Shandong University, 2019GN065 Natural Science Foundation of Shandong Province, ZR2023MA019 Postdoctoral Fellowship Program of China Postdoctoral Science Foundation, GZC20232540 Please add any additional funding sources not stated above:

Thank you for your assistance.

Journal of Applied Physics ARTICLE pubs.aip.org/aip/jap

Strain-controllable electronic, magnetic properties, and magnetic anisotropy energy in a 2D ferromagnetic half-metallic MGT monolayer

Cite as: J. Appl. Phys. **136**, 000000 (2024); doi: 10.1063/5.0239431
Submitted: 22 September 2024 · Accepted: 17 November 2024 ·
Published Online: ■■ ■■ 2024

View Online Export Citation CrossMark

Linhui Lv,[1,2] Fangyu Zhang,[1,2] Diancong Qi,[1,2] Zihao Xu,[3] Weiyi Wang,[4] Ya Su,[5] Yanyan Jiang,[6] and Zhaoyong Guan[1,2,a)]

Q1

AFFILIATIONS

[1]Key Laboratory of Colloid and Interface Chemistry, Ministry of Education, School of Chemistry and Chemical Engineering, Shandong University, Jinan, Shandong 250100, China
[2]School of Chemistry and Chemical Engineering, Shandong University, Jinan 250100, China
[3]School of Physics, Shandong University, Jinan 250100, China
[4]Department of Chemical Physics & Hefei National Laboratory for Physical Sciences at Microscale, University of Science and Technology of China, Hefei, Anhui 230026, China
[5]Key Laboratory for Liquid-Solid Structural Evolution & Processing of Materials (Ministry of Education), School of Materials Science and Engineering, Shandong University, Jinan, Shandong, 250061, China
[6]School of Electrical Engineering, Shandong University, Jinan, Shandong 250100, China

[a)]**Author to whom correspondence should be addressed:** zyguan@sdu.edu.cn

ABSTRACT

The investigation of two-dimensional (2D) intrinsic ferromagnetic material is important in the field of spintronics. In this study, the $Mn_2Ge_2Te_6$ monolayer (ML) with intrinsic ferromagnetism was fabricated by using the density functional theory (DFT). The $Mn_2Ge_2Te_6$ Ml is a half metal (HM) with a spin-β bandgap of 1.462 eV. Biaxial strain could be applied to tune the electronic and magnetic properties of $Mn_2Ge_2Te_6$. The magnetic moment (MM), magnetic exchange parameter (J), band structures, and magnetic anisotropy energy (MAE) could be effectively controlled by the biaxial strains (ε). It originates that the states near the Fermi level mainly come from the contribution of in-plane atomic orbitals. The MM of Mn monotonously increases as the tensile strains increase. The energy difference between different magnetic orders (ΔE) and J also change with the strains. The antiferromagnetic-stripy order always has the lowest energy under the strains. As the strains change, ΔE and J monotonously change as the direct exchange and super-exchange interactions between Mn atoms vary. As the tensile strain decreases and compressive strain increases ($-2.1\% < \varepsilon < 8\%$), the gap of spin-β electrons monotonously decreases. The $Mn_2Ge_2Te_6$ Ml changes from a HM to a normal spin-unpolarized metal under larger compressive strains ($\varepsilon > -2.1\%$). When the tensile strains are applied, the MAE monotonously increases to the largest value of −22.3 meV ($\varepsilon = 12\%$). As the compressive strains increase, the MAE monotonously decreases. Last, the $Mn_2Ge_2Te_6$ Ml changes from an in-plane magnetic anisotropy into a perpendicular magnetic anisotropy under a larger compressive strain (−11%). It origins that the contribution of hybridization between Te's py and pz orbitals to the MAE is changed when the strain changes. Our results offer crucial insights into the potential of strain modulation in a 2D $Mn_2Ge_2Te_6$ Ml, paving the way for future advancements in this field.

Q2

Q3

Journal of Applied Physics ARTICLE pubs.aip.org/aip/jap

I. INTRODUCTION

In recent years, two-dimensional (2D) materials with strong magnetic anisotropy and high Curie temperature (Tc) have received much attention.[1–3] These materials, possessing ultrathin thickness and the absence of dangling surface bonds, exhibit heightened sensitivity to external modulation, facilitating the fine-tuning of their magnetic properties.[4] However, the Mermin–Wagner theory says that 2D magnetic materials cannot exist in the isotropic Heisenberg model at finite temperature.[5] Hence, 2D ferromagnetic (FM) materials are rare to find.[2,6–8] Researchers have used many methods to find more FM materials, increase Tc[9,] and enhance magnetic stability by the processes of modulating[10–12] and synthesizing.[12–15] In recent years, CrI_3,[12,16–20] Fe_3GeTe_2,[2,13,21–25] VS_2,[14,26–29] and $CrGeTe_3$ (CGT) with intrinsic ferromagnetism have been successfully synthesized in the experiments.[15,30–34] Using the density functional theory (DFT), Zhang *et al.* demonstrated that chromium trihalide (SLCT) (CrX_3, X = F, Cl, Br, and I) monolayers (MLs) constitute a series of stable 2D semiconductors with an intrinsic FM order.[17] Further exploration into magnetic anisotropy energy (MAE) was conducted by Webster *et al.* They investigated the strain dependence of the MAE in 2D chromium trihalides CrX_3 (X = Cl, Br, and I) MLs.[19] In a pioneering study, Zhuang *et al.* predicted that a mechanically exfoliated Fe_3GeTe_2 Ml had strong perpendicular magnetic anisotropy (PMA) with a MAE of 0.92 meV/f.u.[22] Furthermore, Kim *et al.* found antiferromagnetic (AFM) coupling induced by oxide formation in the Fe_3GeTe_2 layer,[25] further enriching interfacial effects in these systems. Ma *et al.* found that isotropic strain enhances the magnetic properties of a pristine 2D VX_2 (X = S, Se) ML, with both magnetic moment (MM) and coupling strength increasing accordingly.[28] Chittari *et al.* investigated the electronic and magnetic properties of 2D transition-metal chromium-based phosphates MPX_3 (M = V, Cr, Mn, Fe, Co, Ni, Cu, Zn, and X = S, Se, Te).[14] However, transition metal dichalcogenides (TMDCs) are predominantly nonmagnetic. Researchers have identified CGT as a ferromagnet and demonstrated that strain is an effective method of tuning magnetic properties.[31] Previous studies of CGT were based on defect and compositional engineering or proximity effects, which introduced magnetic response only locally or externally. Therefore, Gong *et al.* investigated the intrinsic long-range FM order in pristine $Cr_2Ge_2Te_6$ atomic layers and achieved unprecedented control over the transition temperature.[15] On the basis of successfully synthesized 2D CrI_3 and CGT, Huang *et al.* made a significant enhancement of ferromagnetism by lowering the virtual exchange gap through heterovalent alloying.[32]

There are relatively few 2D FM materials that have been synthesized, and therefore, in this study, we perform calculations to explore novel materials and uncover their properties. Ideal 2D magnetic materials are expected to have a high Tc,[35] a large MAE,[35,36] controllable electromagnetic properties,[36] and so on. For a half metal (HM),[37] one spin channel is insulating or semiconducting in nature, while the other channel is conducting.[38] As a result, HMs could get 100% spin polarized current.[30] Moreover, HMs are expected to have a higher Tc, and the gap should be large enough to prevent the thermally agitated spin-flip transition and preserve half-metallicity at room temperature.[39] In addition, a large MAE is essential to generate a potential well, to stabilize the process of magnetization in a certain direction (easy magnetization direction) against thermal fluctuations.[40] Therefore, magnetization will not be affected by thermal fluctuation.[1,41] Consequently, a larger MAE is needed.[15,41] In the synthesis of 2D materials, substrates are necessary, but a lattice mismatch between substrates and 2D materials often poses a challenge. Accordingly, strain should be considered.[3,35] Additionally, biaxial strain could effectively control both magnetic and electronic properties, as the states near the Fermi level are predominantly supplied by in-plane atomic orbitals.[42–44] Therefore, we use strain to regulate the magnetic properties in this work.

In this article, we performed a study on the properties of $Mn_2Ge_2Te_6$ (MGT), using the DFT. $Mn_2Ge_2Te_6$ shows an intrinsic FM order, which originates from the super-exchange interaction of the Mn and Ge atoms. $Mn_2Ge_2Te_6$ is a HM, whose spin-β electron is a semiconductor with an indirect gap of 1.462 eV. The magnetic easy axis (EA) prefers to be an in-plane magnetic anisotropy (IMA), originating from indirect spin–orbital coupling (SOC). $Mn_2Ge_2Te_6$ shows good dynamical and thermal stability. Biaxial strain could effectively control the magnetic and electronic properties, as the states near the Fermi level are mainly contributed by in-plane atomic orbitals. Our results indicate that Mn atoms ferromagnetically couple with each other under tensile and compressive strains ($\varepsilon < 10\%$). The energy difference between FM and AFM orders (ΔE) initially decreases, which is attributed to the change in exchange interaction between Mn and Te atoms when the tensile strain increases. The magnetic exchange parameter (J) also changes as the strains change the direct and super-exchange interactions. Additionally, $Mn_2Ge_2Te_6$ could be transferred from a HM to a spin-polarized metal as the compressive strain ($\varepsilon < 2.1\%$) is increased. However, $Mn_2Ge_2Te_6$ is still a HM with a FM order under tensile strains. The MM changes under strains for the different charge transfers. The MM initially increases as the tensile strain increases. $Mn_2Ge_2Te_6$ tends to be an IMA, with a MAE of −13.2 meV/f.u. When the larger compressive strain ($\varepsilon > 11\%$) is applied, the EA could be switched from the [100] to the [001] direction. The EA remains in the plane under tensile strains and compressive strains ($\varepsilon < 11\%$). The MAE monotonously increases as the tensile strain increases. However, the MAE monotonously decreases as the compressive strains increase. It origins that the contribution of hybridization between Te's py and pz orbitals to the MAE is changed when the strain changes. Moreover, $Mn_2Ge_2Te_6$ shows good dynamic stability under strains. Our results provide controllable magnetoelectric properties of $Mn_2Ge_2Te_6$, which are useful for new magnetoelectric devices.

II. COMPUTATIONAL DETAILS

In this study, we performed first-principles calculations within the framework of a spin-polarized DFT using the Vienna *Ab initio* Simulation Package (VASP).[45] Electron exchange interactions were described by the generalized gradient approximation (GGA)[46] parameterized Perdew–Burke–Ernzerhof (PBE) method.[47,48] The Mn's 3d electron was studied with hybrid-functional HSE06[48,49] and the LDA + U method. The energies with different orders, band structures, and density of states (DOS) were calculated by using the HSE06 functional, while the MAE, phonon spectra, and molecular

dynamics were examined by the LDA + U method. Chittari *et al.* investigated carrier- and strain-tunable intrinsic magnetism in two-dimensional MAX_3 transition metal chalcogenides and found that it was appropriate to take the value of U_{eff} as 4 meV.[50] The on-site effective Coulomb interaction parameter (U) was set to 4.60 eV, and the exchange interaction parameter (J_0) was set to 0.60 eV. Accordingly, the effective Ueff (Ueff = U − J0) was 4.00 eV,[30,38] and the corresponding magnetic and electronic properties were consistent with the HSE06 functional. A vacuum space of 16 Å in the z direction was implemented to prevent virtual interaction. The kinetic energy cutoff was set as 300 eV for optimizing the geometry and calculating the energy. The geometries were fully relaxed until energy and force converged to 10^{-6} eV and 1 meV/Å, respectively. Also, 9 × 9 × 1, 16 × 16 × 1 Monkhorst–Pack grids were used for geometry optimization and energy calculation,[51] respectively.

For the calculation of the MAE, we employ a nonlinear mode with the SOC effect. In the MAE calculation, the total energy converges to 1×10^{-8} eV. The MAE is usually small, due to the impact of SOC. Because the calculation of the MAE is sensitive to the parameters, the *k*-mesh test is performed. A 19 × 19 × 1 *k*-mesh is adopted without any symmetric constriction, as shown in Fig. S1 in the supplementary material. The MAE is calculated with an energy cutoff of 400 eV and a total energy convergence of 1×10^{-8} eV. The phonon spectra and DOS are calculated using the finite displacement method as implemented in Phonon Package.[52] A 4 × 4 × 1 cell is adopted in the calculation. The total energy and the Hellmann–Feynman force converges to 10^{-8} eV and 1 meV/Å in the phonon spectra calculation, respectively. Six thousand uniform *k*-points along high-symmetry lines are utilized to obtain phonon spectra.

III. RESULTS AND DISCUSSION

A. Geometry of the $Mn_2Ge_2Te_6$ Ml

We performed GGA calculations to investigate the influence of strain effects on the electromagnetic properties of the $Mn_2Ge_2Te_6$ Ml.[51] Before studying the $Mn_2Ge_2Te_6$ Ml system, we optimized the lattice parameter of $Mn_2Ge_2Te_6$. The optimized geometries of the $Mn_2Ge_2Te_6$ Ml are depicted in top, side 1 (along the x axis) and side 2 (along the y axis) views, as shown in Figs. 1(a), 1(b), and 1(c), respectively. The corresponding optimized lattice parameter (d_1) is a = b = 6.968 Å, which is larger than
Q6 5.989 Å of CGT,[15,53] and 6.881 Å of $Co_2Ge_2Te_6$.[34] It origins that the radius of the Mn atom (137 pm) is larger than that of the Cr (125 pm) and Co atoms (125 pm). The bond length between Mn and Te atoms is 2.915 Å, while the bond length between Ge and Te atoms is 2.617 Å. The bond length between Ge and Ge atoms is 2.477 Å. The distance between the Mn layer and the Ge layer (d_2) is 1.239 Å, while the distance between the Te layer and the Ge layer (d_3) is 3.769 Å. From the optimized geometry, we can find that the $Mn_2Ge_2Te_6$ Ml presents the D_{3d} point group, which is the same with CGT[15] and $Co_2Ge_2Te_6$.[54] Also, we can see that the Mn atom is at the center of the octahedron.

We used a 2 × 2 × 1 supercell, each containing two Mn atoms. Thus, there are two magnetic orders: FM and AFM orders. The total MM of the FM order is 8.00 μ_B, while the AFM order is 0.00 μ_B. The spin charge densities of the FM and AFM orders are

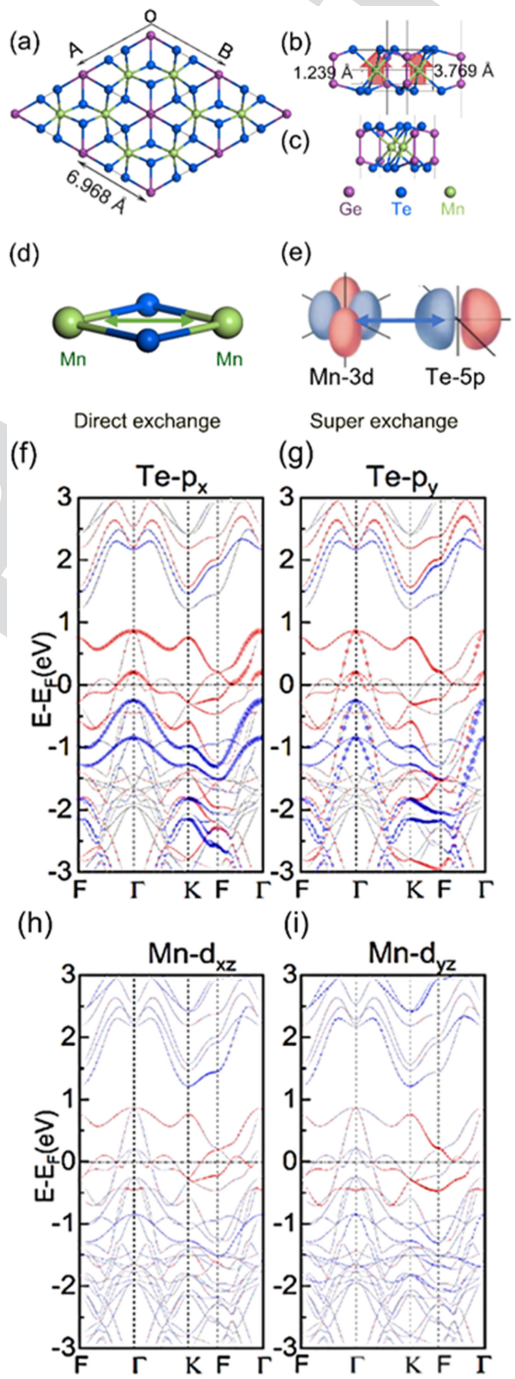

FIG. 1. (a) Top, (b) side 1 (along the x axis), and (c) side 2 (along the y axis) views of optimized geometries of the $Mn_2Ge_2Te_6$ Ml. The purple, blue, and green balls represent Ge, Te, and Mn atoms, respectively. (d) Direct and (e) super-exchange interactions. (f)–(i) The atom projected band structures. (f) Te-p_y, (g) Te-p_x, (h) Mn-d_{xz}, and (i) Mn-d_{yz} projected band structures of the $Mn_2Ge_2Te_6$ Ml. The red and blue lines represent spin-α and spin-β electrons, respectively. The Fermi level is set to 0 eV.

shown in Figs. S2(a)–S2(d) in the supplementary material, respectively. From the spin charge density, we can see that 4.365 μ_B MM is mainly localized in the Mn atom with a high-spin octahedral d^6 configuration, while the MM of the Ge and Te atoms are −0.020 (0.01 × 2) and −0.876 (0.146 × 6) μ_B, respectively. To describe magnetic stability, the ΔE is defined as $\Delta E = EAFM - EFM$. The ΔE is 0.123 eV, indicating that the $Mn_2Ge_2Te_6$ Ml shows the FM order. The ground state is determined by the competition between the direct exchange and the super-exchange interactions, as shown in Figs. 1(d) and 1(e), respectively. In $Mn_2Ge_2Te_6$, the super-exchange interaction is stronger than the direct exchange interaction, and the Mn-*d* and Te-*p* orbitals' super-exchange interaction is dominant in determining the order of $Mn_2Ge_2Te_6$, which is similar to CrI_3 and CGT.[15] The super-exchange interaction arising from the hybridization of the Mn-*d* and Te-*p* orbitals dominates, resulting in a FM order of the $Mn_2Ge_2Te_6$ Ml. The states near the Fermi level are mainly contributed by the Te'*p* orbitals and partially provided by Mn's d*xy* and d*yz* orbitals, shown in Figs. 1(f)–1(i). The energy of the FM and AFM orders changes at different strains, which are shown in Fig. S3 in the supplementary material.

Here, we calculate the Te-p_y, Te-p_x, Mn-d_{xz}, and Mn-d_{yz} projected band structures of the $Mn_2Ge_2Te_6$ Ml, as shown in Figs. 1(f)–1(i), respectively. The partial density of states (PDOS) of Mn atoms' *d* orbitals is also calculated with the HSE06 functional, as shown in Fig. S4 in the supplementary material. The charge densities of the VBM contributed by the spin-β electrons at the Γ point are also calculated with the HSE06 functional, as shown in Fig. S5 in the supplementary material. It can be concluded that the spin-α electrons partially occupy the Fermi level, which implies that its channel is conductive. In contrast, the spin-β electron channel is insulating in nature. Therefore, $Mn_2Ge_2Te_6$ is a HM. There are eight Mn atoms in a 2 × 2 × 1 cell, and the total MM for the FM order amounts to 32.0 μ_B. Moreover, three different AFM orders are considered, including AFM-zigzag (AFM-Z), AFM-stripy (AFM-S), and AFM-Néel (AFM-N) orders. For the AFM order, four Mn atoms have 16.0 μ_B, while the other four Mn atoms have −16.0 μ_B. Consequently, the total MM of the AFM order equals 0.0 μ_B. The spin charge density difference is shown in Fig. S2 in the supplementary material. The highest energy of the AFM-Z order is 0.637 eV higher than the FM order, and the second highest energy of the AFM-N order is 0.614 eV, as shown in Figs. S2(b) and S2(d) in the supplementary material, respectively.

The AFM-stripy (AFM-S) order exhibits an energy of 0.457 eV, which is higher than that of the FM order, as illustrated in Fig. S2(c) in the supplementary material. The corresponding J_1, J_2, and J_3 are 13.6, 7.5, and 12.0 meV for the $Mn_2Ge_2Te_6$ Ml, as shown in Fig. S2(e) in the supplementary material. Both the nearest- and the next-nearest-neighbor Mn atoms exhibit a FM order. It can be concluded that J_3 can be compared with J_1. Similar phenomena occur in other materials such as $NiCl_2$, $NiBr_2$, and NiI_2.[16] Notably, both the nearest-neighbor and the next nearest-neighbor Mn atoms show FM coupling.

Ma *et al.* reported two intrinsically ferromagnetic vdW materials with T_c higher than room temperature, including the T_c of $MnGeTe_3$ up to 349 K. We also calculated that the T_c is about 376 K, as shown in Fig. S6 in the supplementary material, which is in general agreement with this result.[55] The mechanical properties of $Mn_2Ge_2Te_6$ are also investigated. $Mn_2Ge_2Te_6$ is applied with a strain ranging from −10% to 10%. When installing low-dimensional materials on a brittle substrate, bending and stretching strains can be applied experimentally.[56,57] The corresponding strains can be as high up to 10%. In addition, strains can be applied by nanoindentation under atomic force microscopy.[56] Supersaturation strains can be applied using a diamond anvil cell.[58]

B. Magnetization modulation

In-plane strains are often used to modulate magnetism,[59] including the MMs of atoms, the energies of different magnetic orders, and the exchange interaction between magnetic atoms.

In $Mn_2Ge_2Te_6$, the strain can change the atomic MM and enhance or attenuate the FM order. The MMs of various elements constantly change with the direction and magnitude of the applied strains. As shown in Fig. 2(a), the MMs of the Mn and Ge atoms monotonously increase with the strains ($-2\% < \varepsilon < 10\%$). In contrast, the MM of the Te atom monotonously decreases as the

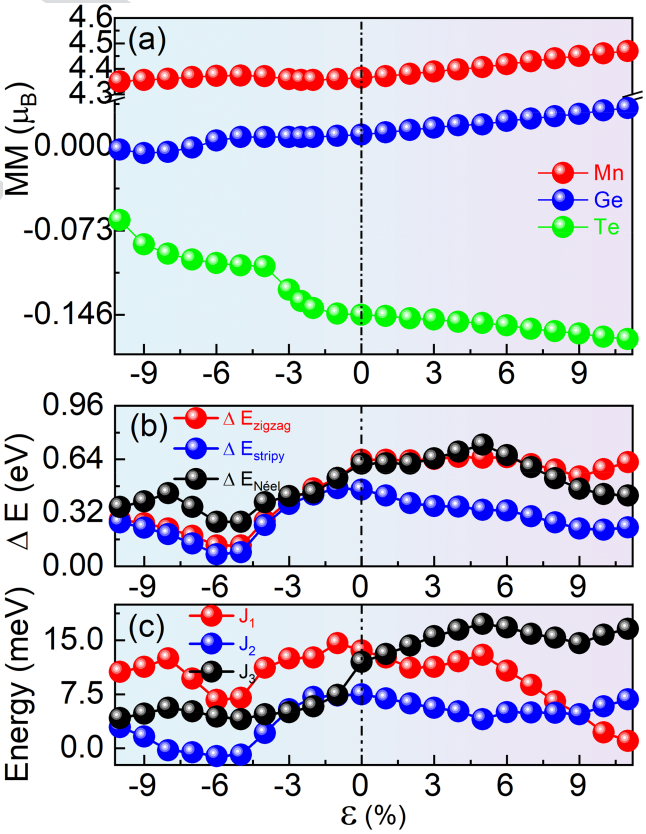

FIG. 2. (a) The MM of the Mn, Ge, and Te atoms change with the biaxial strains. (b) The energy difference between AFM-Z, AFM-S, AFM-N, and FM orders changes with strains. (c) The J_1, J_2, and J_3 change with the biaxial strains.

compressive strain decreases, and it also decreases as the tensile strain increases. The MMs of the Mn, Ge, and Te atoms are (4.389, 0.016, −0.15), (4.418, 0.022, −0.155), and (4.45, 0.028, −0.162) μ_B, respectively, applying compressive strains of −3%, −6%, and −9% to the $Mn_2Ge_2Te_6$ Ml. When the tensile strains of 3%, 6%, and 9% are applied to the $Mn_2Ge_2Te_6$ Ml, the MMs of the Mn, Ge, and Te atoms are (4.356, 0.007, −0.14), (4.373, 0.008, −0.103), and (4.361, −0.005, −0.093) μ_B, respectively. This suggests that the occupation of each atom near the Fermi level varies with strains, as shown in the DOS plot in Fig. S7 in the supplementary material. Simultaneously, the ΔE varies with in-plane strains, as shown in Fig. 2(b). J_1, J_2, and J_3 also vary with the strains, as shown in Fig. 2(c). $Mn_2Ge_2Te_6$ maintains the FM order upon strains, while AFM-stripy still has the second lowest energy. The minimum energy difference between the AFM-stripy and the FM orders ΔEAFM-Stripy (ΔEAFM-Stripy = EAFM-Stripy − EFM) also varies with the strain. The ΔEAFM-Stripy of the $Mn_2Ge_2Te_6$ Ml are 0.372, 0.071, and 0.231 eV, respectively, applying compressive strains of −3%, −6%, and −9%. The ΔEAFM-Néel (ΔEAFM-Néel = EAFM-Néel − EFM) are 0.420, 0.266, and 0.388 eV, respectively, and the ΔEAFM-Zigzag (ΔEAFM-Zigzag = EAFM-Zigzag − EFM) are 0.393, 0.123, and 0.257 eV, respectively. The corresponding J1, J2, and J3 are (12.5, 5.4, 5.0), (6.7, −1.1, 4.4), and (11.3, 1.6, 4.8) meV. When the tensile strains of 3%, 6%, and 9% are applied to the $Mn_2Ge_2Te_6$ Ml, the ΔEAFM-Stripy of the $Mn_2Ge_2Te_6$ Ml are 0.359, 0.334, and 0.225 eV, respectively. The ΔEAFM-Néel are 0.645, 0.664, and 0.463 eV. Also, the ΔEAFM-Zigzag are 0.642, 0.652, and 0.536 eV. The corresponding J1, J2, and J3 are (11.3, 5.6, 15.6), (10.8, 5.0, 16.8), and (4.7, 4.7, 14.6) meV. These findings suggest that in-plane strains can effectively modulate direct exchange and super-exchange interactions.

This is most likely caused by a change in electron occupation in the d orbitals. As shown in Fig. S4 in the supplementary material, we plotted the PDOS of the Mn atom and found that the electron occupancy of the Mn atom's d orbitals changed. We speculate that the strain modulates the MM, direct exchange interaction, and super-exchange interaction.

C. Biaxial strains modulate electronic properties

Biaxial strains are also used to control the electronic properties of 2D materials.[55] ΔE monotonously increases as the tensile strain increases, and $Mn_2Ge_2Te_6$ is a HM under tensile strains. When the tensile stains of 2%, 4%, 6%, 8%, and 10% are applied, the corresponding $d_{Mn\text{-}Mn}$ is 4.130, 4.184, 4.264, 4.345, and 4.425 Å. Under 12% enlarged strain, the corresponding lattice parameter a and $d_{Mn\text{-}Mn}$ are 7.804 and 4.506 Å. As the lattice parameter increases, the corresponding $d_{Mn\text{-}Mn}$ also increases. It means that the direct exchange and super-exchange interactions weaken, causing a decrease of ΔE.

$Mn_2Ge_2Te_6$ maintains the FM order, as ΔE is always negative under strains. This underscores the superior stability of the FM order. ΔE monotonously increases with the application of tensile strains, as shown in Fig. 3(a). ΔE is −133.55 meV without strain, and ΔE is −149.58 meV under 2% tensile strain. When the tensile strain increases to 6%, ΔE is −195.18 meV. ΔE further increases to −214.08 meV under 8% tensile strain. This indicates that the FM order becomes more stable with the application of tensile strains.

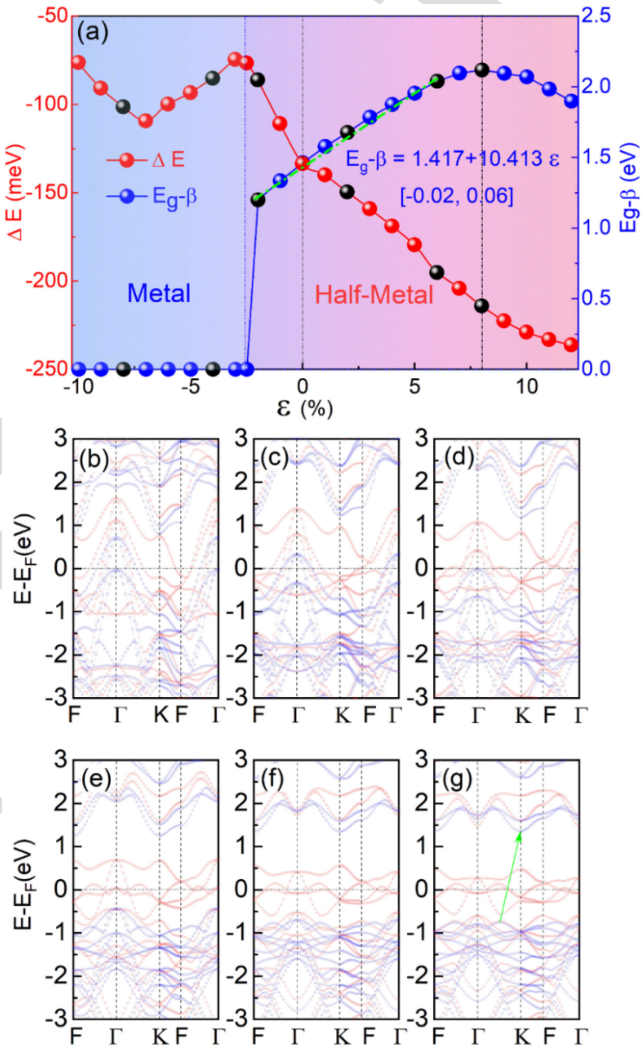

FIG. 3. (a) ΔE between FM and AFM orders and $E_g - \beta$ change with the biaxial strains. (b)–(g) The band structures change with the biaxial strains. The spin-polarized band structures modulated by the strains of (b) −8%, (c) −4%, (d) −2%, (e) 2%, (f) 6%, and (g) 8%, respectively. The red and blue lines represent spin-α and spin-β electrons, respectively.

However, the effects of compressive strains are complex. ΔE is −86.17 meV under −2% compressive strain, while ΔE is −85.25 meV under −4% strain. ΔE is −101.4 meV under −8% compressive strain. ΔE monotonously increases under the strains ($-2.7\% < \varepsilon < 12\%$). In contrast, ΔE monotonously decreases under the strains ($-7\% < \varepsilon < -2.7\%$). When applying larger compressive strains ($-10\% < \varepsilon < -7\%$), ΔE monotonously increases again.

Moreover, strain affects the electronic structure of the $Mn_2Ge_2Te_6$ Ml. The $Mn_2Ge_2Te_6$ Ml is a HM with $E_g - \beta$ of 1.462 eV without strain. The band structures change with the biaxial strains, as

shown in Figs. 3(b)–3(g). $E_g - \beta$ changes with tensile strain, while $Mn_2Ge_2Te_6$ is always a HM. $E_g - \beta$ is 1.244 eV under 2% tensile strain, as shown in Fig. 3(e). $E_g - \beta$ increases to 1.342 eV when 6% tensile strain is applied, as shown in Fig. 3(f). $E_g - \beta$ follows the relationship $Eg - \beta = 1.417 + 10.413$varepsilon$(-0.02 \leq \varepsilon \leq 0.06)$. $E_g - \beta$ is 1.359 eV, under 8% tensile strain, as shown in Fig. 3(g). When −2% compressive strain is applied, $E_g - \beta$ is 1.185 eV, and $Mn_2Ge_2Te_6$ remains a HM, as shown in Fig. 3(d). When −2.7% compressive strain is applied, $E_g - \beta$ becomes 0 eV and the $Mn_2Ge_2Te_6$ Ml transforms into metal. $E_g - \beta$ remains 0 eV, when compressive strains $(-10\% < \varepsilon < -2.7\%)$ are applied, as shown in Figs. 3(b) and 3(c), respectively. This suggests that the occupation of each atom near the Fermi level varies with strains, as shown in Fig. S7 in the supplementary material.

D. Magnetic anisotropy properties and MAE modulation

The shift of the MM from a soft axis (EA) to a hard axis necessitates energy expenditure to overcome the "energy barrier."[36] This required energy is referred to as MAE.[41] Materials with high MAE demonstrate enhanced magnetic stability.[60]

The lattice parameters of the material can be changed by applying strain, thereby changing the magnetic anisotropy.[61] Consequently, in-plane strain is widely used to modulate the MAE of 2D materials.[60] The MAE changes with different strains, as shown in Figs. 4(a)–4(e). When strains are applied to $Mn_2Ge_2Te_6$, $\Delta E0$ $(\Delta E0 = E - E[001])$ is used to describe the MAE. The $\Delta E0$ changes with θ, following this equation:

$$\Delta E_0 = K_1 \cos^2\theta + K_2 \cos^4\theta + K_3 \cos^6\theta. \quad (1)$$

K_1 and K_2 denote the contribution of the quadratic and quartic parts to the MAE, respectively.K_3 approximately equals 0, which could be negligible. Hence, Eq. (1) is simplified into the following equation:

$$\Delta E_0 = K_1 \cos^2\theta + K_2 \cos^4\theta. \quad (2)$$

When −10% and −6% strains are applied, the $\Delta E0$ could be calculated by using the following equations: ΔE_0 (meV) $= -0.603\cos^2\theta + 0.027\cos^4\theta$ and ΔE_0 (meV) $= -7.17\cos^2\theta + 1.50\cos^4\theta$. The corresponding MAEs are −0.546 and −5.63 meV/f.u. When the tensile strains of 6% and 10% are applied, the ΔE_0 could be obtained from the following equations: ΔE_0 (meV) $= -14.4\cos^2\theta - 1.14\cos^4\theta$ and ΔE_0 (meV) $= -3.3\cos^2\theta - 0.359\cos^4\theta$. The corresponding MAEs are −15.71 and −18.49 meV/f.u. Also, we calculate that the EA direction of $MnGeTe_3$ is along the [100] direction, and the MAE of $MnGeTe_3$ is about 13 204 μV, which is the same as the calculations of Chittari *et al.*[50]

MAE is important for the storage of magnetic information, while PMA is of great significance.[62,63] To clarify the switch of the EA, it is necessary to determine the contribution of each atomic orbital to the MAE of $Mn_2Ge_2Te_6$. Furthermore, explaining the relationship between MAEs and strains is paramount. Tight binding and second-order perturbation theory are used to calculate

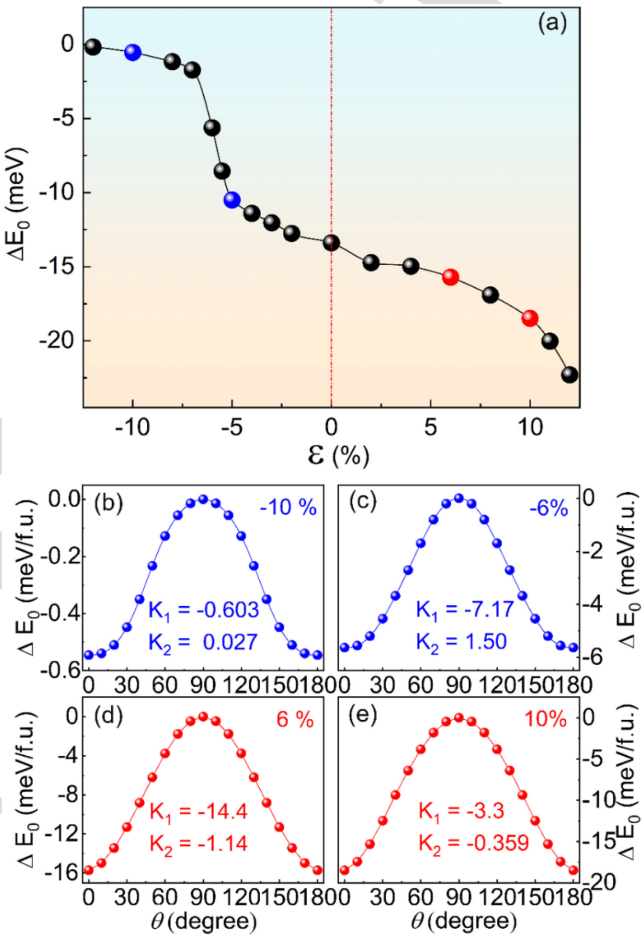

FIG. 4. (a) MAEs change with the biaxial strains. The energy varies as a function of the polar angle θ of magnetization for the $Mn_2Ge_2Te_6$ Ml. The energy varies with different in-plane strains of (b) −10%, (c) −6%, (d) 6%, and (e) 10%, respectively.

MAE. According to the canonical formula, each atom's contribution to MAE can be calculated by using the following formula:[34,36]

$$\mathrm{MAE_i} = \left[\int E_f(E - E_F)[n_i^{[100]}(E) - n_i^{[001]}(E)]\right], \quad (3)$$

where $\mathrm{MAE_i}$ presents the MAE contributed by atom i. $n_i^{[100]}$ and $n_i^{[001]}$ mean the DOS with the EA along the [100] and [001] directions, respectively. The following formula is used to calculate the total MAE:

$$\mathrm{MAE_{tot}} = \sum_i \mathrm{MAE_i}, \quad (4)$$

where $\mathrm{MAE_{tot}}$ is the sum of $\mathrm{MAE_i}$. Given the second-order perturbation theory, the MAE can be calculated by using the following

Journal of Applied Physics ARTICLE pubs.aip.org/aip/jap

TABLE I. The matrix differences for *d* orbitals between magnetization along the [001] and [100] directions in Eqs. (5) and (6).

	o^+					o^-				
u^-	d_{xy}	d_{yz}	d_{z^2}	d_{xz}	$d_{x^2-y^2}$	d_{xy}	d_{yz}	d_{z^2}	d_{xz}	$d_{x^2-y^2}$
d_{xy}	0	0	0	1	−4	0	0	0	−1	4
d_{yz}	0	0	3	−1	1	0	0	−3	1	−1
d_{z^2}	0	3	0	0	0	0	−3	0	0	0
d_{xz}	1	−1	0	0	0	−1	1	0	0	0
$d_{x^2-y^2}$	−4	1	0	0	0	4	−1	0	0	0

equations:

$$\Delta E^{--} = E_x^{--} - E_z^{--} = \xi^2 \sum_{o^+,u^-} (|<o^-|L_z|u^-|^2 - |<o^-|L_x|u^->|^2)/(E_u^- - E_o^-), \tag{5}$$

$$\Delta E^{-+} = E_x^{+-} - E_z^{+-} = \xi^2 \sum_{o^+,u^-} (|<o^+|L_z|u^-|^2 - |<o^+|L_x|u^->|^2)/(E_u^- - E_o^-), \tag{6}$$

where + and − mean spin-α and spin-β states, and ξ, L_x, and L_z represent the SOC constant and angular momentum operators in the [100] and [001] directions, respectively. *u* and *o* represent unoccupied and occupied states, respectively. E_u and E_o represent the energies of unoccupied and occupied states, respectively. The MAE is primarily composed of spin orbital matrix elements and energy differences. The MAE is related to the DOS near the Fermi level. The matrix element differences $|<o^-|L_z|u^-|^2 - |<o^-|L_x|u^->|^2$ and $|<o^+|L_z|u^-|^2 - |<o^+|L_x|u^->|^2$ of the *d* and *p* orbitals are calculated, as shown in Tables I and II, respectively. In order to clarify Mn's contribution to the MAE, the matrix differences for the *d* orbitals, including the d_{xy}, d_{yz}, d_{z^2}, d_{xz}, and $d_{x^2-y^2}$ orbitals between the EA along the [100] and [001] directions are calculated, as shown in Table I.

To further explain the variation of the MAE with strains, we also calculated the atomic orbital decomposition MAE, as shown in Figs. 5(a)–5(i). It can be concluded that the MAE partly comes from Mn [Figs. 5(a)–5(c)] and Ge atom contributions [Figs. 5(d)–5(f)] but mainly from Te atom contributions [Figs. 5(g)–5(i)].

TABLE II. The matrix differences for *p* orbitals between the EA along the [001] and [100] directions in Eqs. (5) and (6).

	o^+			o^-		
u^-	p_y	p_z	p_x	p_y	p_z	p_x
p_y	0	1	−1	0	−1	1
p_z	1	0	0	−1	0	0
p_x	−1	0	0	1	0	0

Wang. *et al.* investigated the ferroelectric control of magnetic anisotropy in a multiferroic heterostructure $EuSn_2As_2/In_2Se_3$ and found that the f(p) orbitals of Eu (Sn and As) atoms were the primary contributors to the SOC-MAE.[64] They found that the contributions from the As and the Sn atoms stemmed from the inter-orbital couplings between p*y* and p*z* orbitals, as well as between p*x* and p*y* orbitals, which are similar with our results. The orbital-resolved MAE of intrinsic $Mn_2Ge_2Te_6$ without strain is shown in Figs. 5(a), 5(d) and 5(g). The total MAE is −13.40 meV/f.u. Te atoms provide −11.95 meV/f.u. In addition, the Te atoms of $Mn_2Ge_2Te_6$ contribute −11.76 (2.94 × 4) meV/f.u. to the total MAE, while Mn and Ge atoms' contribution could be negligible. However, Cr atoms provide 0.06 (0.03 × 2) meV/f.u. The Te atoms supply 0.12 (0.03 × 4) and Ge atoms provide −0.050 (−0.025 × 2) meV/f.u. to the total MAE of the CGT ML.[65] Thus, the MAE of $Mn_2Ge_2Te_6$ is larger than CGT. When 6% strain is applied, the hybridizations between Mn's *d* orbital and Ge's *p* orbital are similar, with neutral $Mn_2Ge_2Te_6$, as shown in Figs. 5(b) and 5(e). However, the hybridization between Te's *p* orbitals changes, totally providing −15. 01 meV/f.u. The contribution of hybridization between Te's p*y* and p*z* decreases to −18.36 meV/f.u., as shown in Fig. 5(h). Correspondingly, the MAE increases to −15.71 meV/f.u., as shown in Fig. 4(a). When −6% strain is applied to $Mn_2Ge_2Te_6$, the orbital-resolved MAE of $Mn_2Ge_2Te_6$ is shown in Figs. 5(c), 5(f) and 5(i). Specifically, the hybridizations between Te's p*x* and p*z* orbitals and p*y* and p*z* orbitals get weakened, as shown in Fig. 5(i). Consequently, their contribution to the total MAE reduces to −5.28 meV/f.u. Eventually, the MAE decreases to −5.63 meV/f.u., as shown in Fig. 4(a).

Meanwhile, matrix differences for the *p* orbitals are calculated to clarify the Ge and Te atoms' contribution to the MAE. The matrix differences for the *p* orbitals, including the p*y*, p*z*, and p*x* orbitals between the EA along the [100] and [001] directions are calculated, as shown in Table II.

As a result, we can see that the hybridization of the Mn d*yz* and dz^2 orbitals makes positive contributions to the MAE, resulting in a matrix difference of 3 for the *d* orbitals, as shown in Table I. The hybridization of the d*xy* and $d_{x^2-y^2}$ orbitals makes a negative contribution to the MAE, corresponding to a matrix difference of −4 for the *d* orbital. Compared with the $Co_2Ge_2Te_6$ Ml, the hybridization between Co's d*xy* and $d_{x^2-y^2}$ orbitals makes a negative contribution to the MAE (−0.22 and −0.15 meV), which corresponds to the matrix differences of −3 and −4 for the *d* orbitals, respectively.[34] The Ge atoms' contribution to the MAE is negligible compared with that of the Te atoms. The hybridization between the spin-β-occupying p_y and the spin-β-occupying p*z*orbital of Te is beneficial for the IMA (negative value), corresponding to the matrix difference of −1 for the *p* orbital. However, the hybridization between the spin-β-occupying p*z* and the spin-β p*x* orbital is beneficial for the PMA (positive value), corresponding to the matrix 1 for the *p* orbital, as shown in Table II. In general, the total MAE is almost dominated by the hybridization between Te's p*y* and p*z* orbitals.

E. Dynamic stability

The phonon band structure and DOS of the $Mn_2Ge_2Ge_6$ Ml is also calculated with the LDA + U method, as shown in Fig. S8

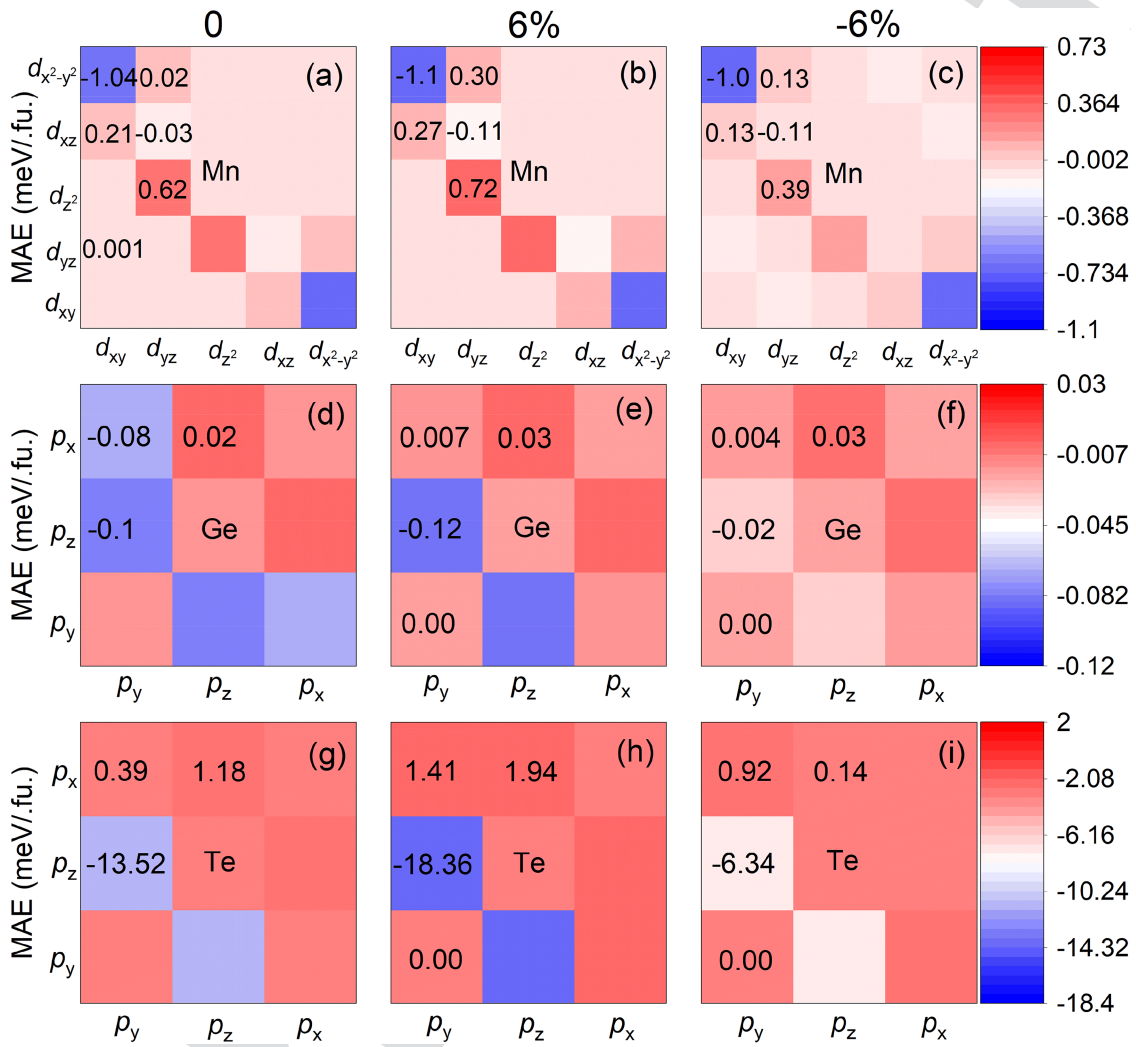

FIG. 5. Orbital-resolved MAE of $Mn_2Ge_2Te_6$ with biaxial strains of 0, 6%, and −6%, respectively. The orbital-resolved MAE of $Mn_2Ge_2Te_6$ changes with strains of (a), (d), and (g) 0, (b), (e), and (h) 6%, and (c), (f), and (i) −6%, respectively.

in the supplementary material. The dynamic stability of $Mn_2Ge_2Te_6$ after applied strain is confirmed by the phonon dispersion curves and phonon DOS,[39] with no obvious virtual phonon modes, as shown in Figs. 6(a)–6(h). For instance, considering the application of 6% tensile strain and −6% compressive strain, the highest vibrational frequencies are 7.389 and 8.135 THz, respectively, as shown in Figs. 6(a) and 6(e). From Figs. 6(b), 6(d), 6(f), and 6(h), we can see that at low frequencies (0ltε < 3 THz), the contribution mainly comes from Te atoms, while Ge atoms make a higher contribution to the high frequency (6ltε < 8 THz). The main contribution of the Mn atoms is to the intermediate frequency (4ltε < 5 THz). This result corresponds to that of the phonon band. We find that the $Mn_2Ge_2Te_6$ under different strains are thermodynamically stable, resulting from their lowest frequencies are above 0. The highest frequency of intrinsic $Mn_2Ge_2Te_6$ is 7.39 THz, while these values are 7.36 (9%) and 7.39 THz (6%) under tensile strains, respectively. In contrast, the highest frequencies of $Mn_2Ge_2Te_6$ are 8.60 (−9%) and 8.14 THz (−6%) under compressive strains, respectively. The highest phonon frequency corresponds to the frequency of the telescopic vibration, which is related to the bonding level.

Thus, the highest phonon frequency is related to its thermal conductivity. A higher telescopic vibration frequency indicates a stronger bond level and enhanced thermal conductivity. Therefore, we find that compressive strain improves the thermal conductivity of the $Mn_2Ge_2Te_6$ Ml.

Journal of Applied Physics ARTICLE pubs.aip.org/aip/jap

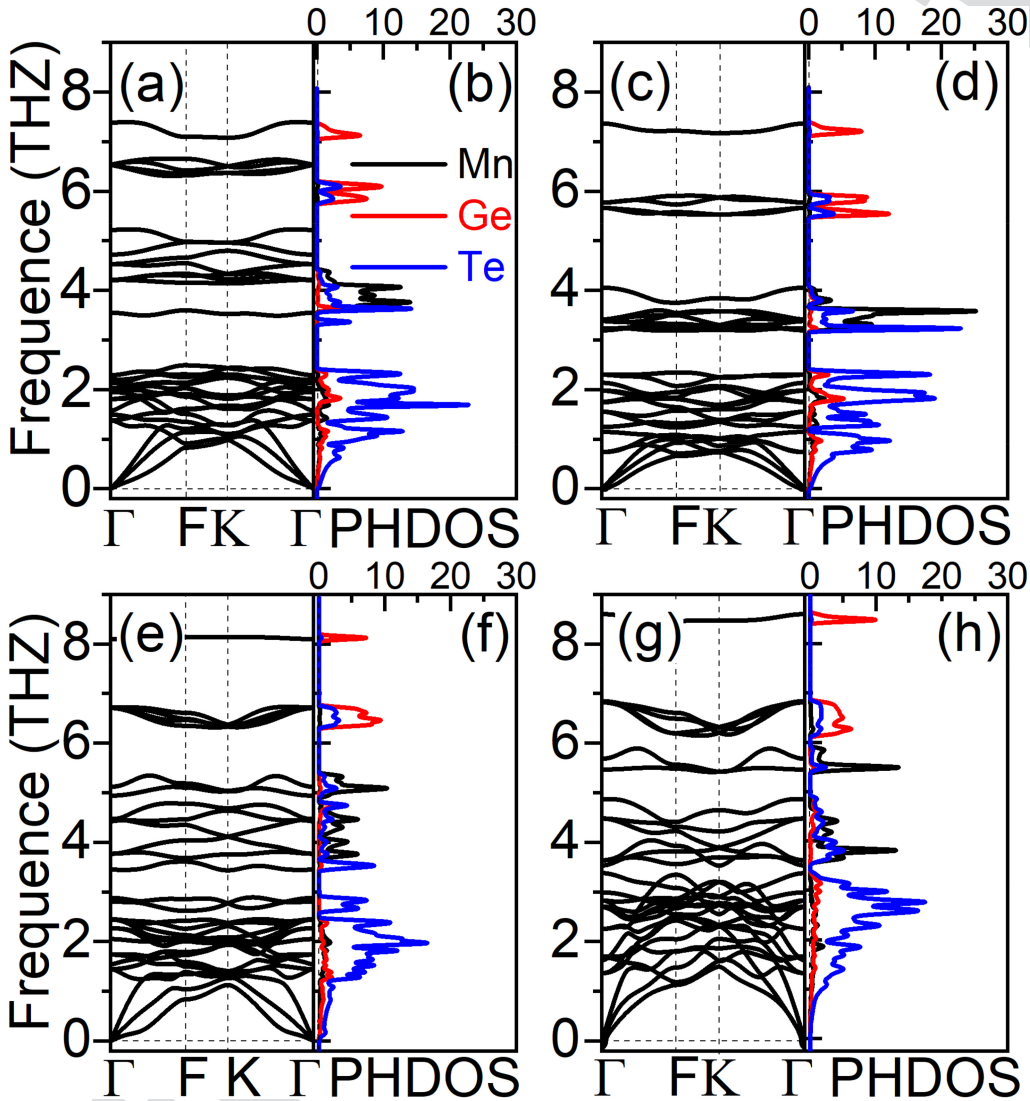

FIG. 6. (a), (c), (e), and (g). The phonon band structures and (b), (d), (f), and (h) DOS of the $Mn_2Ge_2Te_6$ Ml. The phonon band structure under the biaxial strains of (a) +6%, (c) +9%, (e) −6%, and (g) −9%, and the corresponding phonon DOS are calculated with the LDA + U method.

IV. CONCLUSION

In summary, our investigation delved into the strain modulation of the electromagnetic state and its impact on the magnetic anisotropy of the $Mn_2Ge_2Te_6$ Ml under in-plane compressive and tensile strains, employing the DFT. We found the intrinsic ferromagnetism of the $Mn_2Ge_2Te_6$ Ml, which arises from superexchange interactions between Mn and Te atoms. We explored the electronic and magnetic properties of $Mn_2Ge_2Te_6$ across in-plane strain rates ranging from 10% to −10%. The $Mn_2Ge_2Te_6$ Ml shows a HM under tensile strains, while it can be transferred into a spin-polarized metal under compressive strains. Notably, while $Mn_2Ge_2Te_6$ maintains the FM order, strain induces a notable alteration in its MM, J, and MAE. This phenomenon shows the sensitivity of MAE to variations of strain, as the contribution of hybridization between Te's p*y* and p*z* orbitals to the MAE changes. Meanwhile, $Mn_2Ge_2Te_6$ always shows good dynamic stability, under both compressive and tensile strains. This effective manipulation of $Mn_2Ge_2Te_6$ Ml magnetism through strain application holds promise for broadening its applications in spintronics.

SUPPLEMENTARY MATERIAL

See the supplementary material for the convergence of MAE is tested with different *k*-meshes, spin charge density differences and exchange interactions, energy with FM and AFM orders

calculated with the HSE06 functional, the Mn *d* orbitals' PDOS of the $Mn_2Ge_2Te_6$ Ml, the charge densities of the VBM of spin-β electrons at the Γ point calculated with the HSE06 functional, the Mn orbitals' PDOS under strains of −8%, −4%, −2% 3%, 6%, and 9%, the phonon band structure and DOS of the $Mn_2Ge_2Te_6$ Ml calculated with the LDA + U method, and the phonon band structure and DOS of the CGT ML calculated with the LDA + U method.

ACKNOWLEDGMENTS

This work received financial support from the Natural Science Foundation of China (Grant No. 11904203), the Fundamental Research Funds of Shandong University (Grant No. 2019GN065), and the Natural Science Foundation of Shandong Province (ZR2023MA019). Dr. Weiyi Wang acknowledges the Postdoctoral Fellowship Program of China Postdoctoral Science Foundation (No. GZC20232540) and is grateful for the computational resources available at the Shanghai Supercomputer Center. The scientific calculations in this paper have been performed on the HPC Cloud Platform of Shandong University. The authors are grateful to Beijing Beilong Super Cloud Computing Co., Ltd for providing the computation resource at the Beijing Super Cloud Computing Center. The numerical calculations in this paper have been done at the Hefei Advanced Computing Center.

AUTHOR DECLARATIONS

Conflict of Interest

The authors have no conflicts to disclose.

Author Contributions

Linhui Lv: Conceptualization (lead); Data curation (lead); Investigation (lead); Software (equal); Writing – original draft (lead). **Fangyu Zhang:** Data curation (supporting); Formal analysis (supporting). **Diancong Qi:** Data curation (supporting); Formal analysis (supporting); Software (supporting). **Zihao Xu:** Data curation (supporting); Software (supporting). **Weiyi Wang:** Data curation (supporting); Formal analysis (supporting). **Ya Su:** Data curation (supporting); Formal analysis (supporting). **Yanyan Jiang:** Validation (supporting). **Zhaoyong Guan:** Project administration (lead); Supervision (lead); Validation (lead); Writing – review & editing (lead).

DATA AVAILABILITY

The data that support the findings of this study are available from the corresponding author upon reasonable request.

REFERENCES

[1]Y. P. Feng, L. Shen, M. Yang, A. Wang, M. Zeng, Q. Wu, S. Chintalapati, and C.-R. Chang, "Prospects of spintronics based on 2D materials," Wiley Interdiscip. Rev.: Comput. Mol. Sci. **7**, 1759 (2017). Q8

[2]M. Gibertini, M. Koperski, A. F. Morpurgo, and K. S. Novoselov, "Magnetic 2D materials and heterostructures," Nat. Nanotechnol. **14**, 408 (2019).

[3]P. Huang, P. Zhang, S. Xu, H. Wang, X. Zhang, and H. Zhang, "Recent advances in two-dimensional ferromagnetism: Materials synthesis, physical properties and device applications," Nanoscale **12**, 2309 (2020).

[4]N. Zhou, R. Yang, and T. Zhai, "Two-dimensional non-layered materials," Mater. Today Nano **8**, 100051 (2019).

[5]N. D. Mermin and H. Wagner, "Absence of ferromagnetism or antiferromagnetism in one- or two-dimensional isotropic Heisengerg models," Phys. Rev. Lett. **17**, 1133 (1966).

[6]S. Z. Butler, S. M. Hollen, L. Cao, Y. Cui, J. A. Gupta, H. R. Gutiérrez, T. F. Heinz, S. S. Hong, J. Huang, A. F. Ismach *et al.*, "Progress, challenges, and opportunities in two-dimensional materials beyond graphene," ACS Nano **7**, 2898 (2013).

[7]K. S. Novoselov, A. Mishchenko, A. Carvalho, and A. H. Castro Neto, "2D materials and van der Waals heterostructures," Sci. Adv. **353**, 6298 (2016).

[8]E. C. Ahn, "2D materials for spintronic devices," npj 2D Mater. Appl. **4**, 17 (2020).

[9]S. Chen, C. Huang, H. Sun, J. Ding, P. Jena, and E. Kan, "Boosting the curie temperature of Two-dimensional semiconducting CrI_3 monolayer through van der Waals heterostructures," J. Phys. Chem. C **123**, 17987 (2019).

[10]S. Jiang, L. Li, Z. Wang, K. F. Mak, and J. Shan, "Controlling magnetism in 2D CrI3 by electrostatic doping," Nat. Nanotechnol. **13**, 549 (2018).

[11]M. Rassekh, J. He, S. Farjami Shayesteh, and J. J. Palacios, "Remarkably enhanced curie temperature in monolayer CrI3 by hydrogen and oxygen adsorption: A first-principles calculations," Comput. Mater. Sci. **183**, 109820 (2020).

[12]B. Huang, G. Clark, D. R. Klein, D. MacNeill, E. Navarro-Moratalla, K. L. Seyler, N. Wilson, M. A. McGuire, D. H. Cobden, D. Xiao *et al.*, "Electrical control of 2D magnetism in bilayer CrI_3," Nat. Nanotechnol. **13**, 544 (2018).

[13]Z. Fei, B. Huang, P. Malinowski, W. Wang, T. Song, J. Sanchez, W. Yao, D. Xiao, X. Zhu, A. F. May *et al.*, "Two-dimensional itinerant ferromagnetism in atomically thin Fe_3GeTe_2," Nat. Mater. **17**, 778 (2018).

[14]B. L. Chittari, Y. Park, D. Lee, M. Han, A. H. MacDonald, E. Hwang, and J. Jung, "Electronic and magnetic properties of single-layer MPX_3 metal phosphorous trichalcogenides," Phys. Rev. B **94**, 18 (2016).

[15]C. Gong, L. Li, Z. Li, H. Ji, A. Stern, Y. Xia, T. Cao, W. Bao, C. Wang, Y. Wang *et al.*, "Discovery of intrinsic ferromagnetism in two-dimensional van der Waals crystals," Nat. Chem. **546**, 265 (2017).

[16]J. Y. Ni, X. Y. Li, D. Amoroso, X. He, J. S. Feng, E. J. Kan, S. Picozzi, and H. J. Xiang, "Giant biquadratic exchange in 2D magnets and its role in stabilizing ferromagnetism of $NiCl_2$ monolayers," Phys. Rev. Lett. **127**, 247204 (2021).

[17]W. B. Zhang, Q. Qu, P. Zhu, and C. H. Lam, "Robust intrinsic ferromagnetism and half semiconductivity in stable two-dimensional single-layer chromium trihalides," J. Mater. Chem. C **3**, 12457 (2015).

[18]J. L. Lado and J. Fernández-Rossier, "On the origin of magnetic anisotropy in two dimensional CrI_3," 2D Mater. **4**, 035002 (2017).

[19]L. Webster and J. A. Yan, "Strain-tunable magnetic anisotropy in monolayer $CrCl_3$, $CrBr_3$, and CrI_3," Phys. Rev. B **98**, 144411 (2018).

[20]D. Zhong, K. L. Seyler, X. Y. Linpeng, R. Cheng, N. Sivadas, B. Huang, E. Schmidgall, T. Taniguchi, K. Watanabe, M. A. McGuire *et al.*, "Van der Waals engineering of ferromagnetic semiconductor heterostructures for spin and valleytronics," Sci. Adv. **3**, e1603113 (2017).

[21]X. Jiang, Q. X. Liu, J. P. Xing, N. S. Liu, Y. Guo, Z. F. Liu, and J. J. Zhao, "Recent progress on 2D magnets: Fundamental mechanism, structural design and modification," Appl. Phys. Rev. **8**, 031305 (2021).

[22]H. L. L. Zhuang, P. R. C. Kent, and R. G. Hennig, "Strong anisotropy and magnetostriction in the two-dimensional Stoner ferromagnet Fe_3GeTe_2," Phys. Rev. B **93**, 134407 (2016).

[23]X. Wang, J. Tang, X. X. Xia, C. L. He, J. W. Zhang, Y. Z. Liu, C. H. Wan, C. Fang, C. Y. Guo, W. L. Yang *et al.*, "Current-driven magnetization switching in a van der Waals ferromagnet Fe_3GeTe_2," Sci. Adv. **5**, eaaw8904 (2019).

[24]Y. J. Deng, Y. J. Yu, Y. C. Song, J. Z. Zhang, N. Z. Wang, Z. Y. Sun, Y. F. Yi, Y. Z. Wu, S. W. Wu, J. Y. Zhu *et al.*, "Gate-tunable room-temperature ferromagnetism in two-dimensional Fe_3GeTe_2," Nat. Chem. **563**, 94 (2018).

[25]D. Kim, S. Park, J. Lee, J. Yoon, S. Joo, T. Kim, K. J. Min, S. Y. Park, C. Kim, K. W. Moon *et al.*, "Antiferromagnetic coupling of van der Waals ferromagnetic Fe_3GeTe_2," Nanotechnology **30**, 245701 (2019).

[26]C. M. Zhang, Y. H. Nie, S. Sanvito, and A. J. Du, "First-principles prediction of a room-temperature ferromagnetic Janus VSSe monolayer with piezoelectricity, ferroelasticity, and large valley polarization," Nano Lett. **19**, 1366 (2019).
[27]Y. Q. Guo, H. T. Deng, X. Sun, X. L. Li, J. Y. Zhao, J. C. Wu, W. S. Chu, S. J. Zhang, H. B. Pan, X. S. Zheng *et al.*, "Modulation of metal and insulator states in 2D ferromagnetic VS_2 by van der Waals interaction engineering," Adv. Mater. **29**, 1700715 (2017).
[28]Y. D. Ma, Y. Dai, M. Guo, C. W. Niu, Y. T. Zhu, and B. B. Huang, "Evidence of the existence of magnetism in pristine VX_2 monolayers (X = S, Se) and their strain-induced tunable magnetic properties," ACS Nano **6**, 1695 (2012).
[29]H. R. Fuh, C. R. Chang, Y. K. Wang, R. F. L. Evans, R. W. Chantrell, and H. T. Jeng, "Newtype single-layer magnetic semiconductor in transition-metal dichalcogenides VX_2 (X = S, Se and Te)," Sci. Rep. **6**, 32625 (2016).
[30]S. J. Gong, C. Gong, Y. Y. Sun, W. Y. Tong, C. G. Duan, J. H. Chu, and X. Zhang, "Electrically induced 2D half-metallic antiferromagnets and spin field effect transistors," PNAS **115**, 8511 (2018).
[31]N. Sivadas, M. W. Daniels, R. H. Swendsen, S. Okamoto, and D. Xiao, "Magnetic ground state of semiconducting transition-metal trichalcogenide monolayers," Phys. Rev. B **91**, 235425 (2015).
[32]C. X. Huang, J. S. Feng, F. Wu, D. Ahmed, B. Huang, H. J. Xiang, K. M. Deng, and E. J. Kan, "Toward intrinsic room-temperature ferromagnetism in two-dimensional semiconductors," J. Am. Chem. Soc. **140**, 11519 (2018).
[33]Z. Y. Guan, L. H. Lv, Z. Y. An, Y. Y. Jiang, and Y. Su, "Tailing the magnetoelectric properties of $Cr_2Ge_2Te_6$ by engineering covalently bonded Cr self-intercalation: Ferromagnetic half-metal," ACS Appl. Electron. Mater. **5**, 2999 (2023).
[34]Z. Y. Guan, L. H. Lv, Z. Y. An, Y. Su, Y. Y. Jiang, X. M. Wu, and S. Ni, "Van der Waals stacked 2D-layered $Co_2Ge_2Te_6$ with high Curie temperature and large magnetic crystal anisotropy," J. Phys. Chem. C **127**, 5991 (2023).
[35]Z. Guan and S. Ni, "Strain-controllable high Curie temperature and magnetic crystal anisotropy in a 2D ferromagnetic semiconductive FeI_3 monolayer," ACS Appl. Electron. Mater. **3**, 3147 (2021).
[36]Z. Guan and S. Ni, "Prediction of high curie temperature, large magnetic crystal anisotropy, and carrier doping-induced half-metallicity in two-dimensional ferromagnetic FeX_3 (X = F, Cl, Br, and I) monolayers," J. Phys. Chem. C **125**, 16700 (2021).
[37]R. A. de Groot, F. M. Mueller, P. G. van Engen, and K. H. J. Buschow, "New class of materials: Half-metallic ferromagnets," Phys. Rev. Lett. **50**, 2024 (1983).
[38]X. X. Li and J. L. Yang, "First-principles design of spintronics materials," Natl. Sci. Rev. **3**, 365 (2016).
[39]Z. An, Y. Su, S. Ni, and Z. Guan, "Carrier doping modulates 2D intrinsic ferromagnetic $Mn_2Ge_2Te_6$ monolayer, high curie temperature, large magnetic crystal anisotropy," J. Phys. Chem. C **126**, 11330 (2022).
[40]S. Azevedo, J. R. Kaschny, C. M. C. de Castilho, and F. de Brito Mota, "A theoretical investigation of defects in a boron nitride monolayer," Nanotechnology **18**, 495707 (2007).
[41]P. Błoński and J. Hafner, "Magnetic anisotropy of transition-metal dimers: Density functional calculations," Phys. Rev. B **79**, 224418 (2009).
[42]H. J. Jiang, L. Zheng, Z. Liu, and X. W. Wang, "Two-dimensional materials: From mechanical properties to flexible mechanical sensors," Infomat **2**, 1077 (2020).
[43]G. G. Naumis, S. Barraza-Lopez, M. Oliva-Leyva, and H. Terrones, "Electronic and optical properties of strained graphene and other strained 2D materials: A review," Rep. Prog. Phys. **80**, 096501 (2017).
[44]M. A. Bissett, M. Tsuji, and H. Ago, "Strain engineering the properties of graphene and other two-dimensional crystals," Phys. Chem. Chem. Phys. **16**, 11124 (2014).
[45]G. Kresse and J. Furthmüller, "Efficiency of ab-initio total energy calculations for metals and semiconductors using a plane-wave basis set," Comput. Mater. Sci. **6**, 15 (1996).
[46]A. Liechtenstein, V. I. Anisimov, and J. Zaanen, "Density-functional theory and strong interactions: Orbital ordering in Mott-Hubbard insulators," Phys. Rev. B **52**, R5467 (1995).
[47]J. P. Perdew, K. Burke, and M. Ernzerhof, "Generalized gradient approximation made simple," Phys. Rev. Lett. **77**, 3865 (1996).
[48]J. P. Perdew, K. Burke, and M. Ernzerhof, "Generalized gradient approximation made simple," Phys. Rev. Lett. **78**, 1396 (1997).
[49]J. Heyd, G. E. Scuseria, and M. Ernzerhof, "Hybrid functionals based on a screened Coulomb potential," J. Chem. Phys. **118**, 8207 (2003).
[50]B. L. Chittari, D. Lee, N. Banerjee, A. H. MacDonald, E. Hwang, and J. Jung, "Carrier- and strain-tunable intrinsic magnetism in two-dimensional MAX3 transition metal chalcogenides," Phys. Rev. B **101**, 2469 (2020).
[51]H. J. Monkhorst and J. D. Pack, "Special points for Brillouin-zone integrations," Phys. Rev. B **13**, 5188 (1976).
[52]A. Togo and I. Tanaka, "First principles phonon calculations in materials science," Scr. Mater. **108**, 1 (2015).
[53]J. He, G. Ding, C. Zhong, S. Li, D. Li, and G. Zhang, "Remarkably enhanced ferromagnetism in a super-exchange governed $Cr_2Ge_2Te_6$ monolayer via molecular adsorption," J. Mater. Chem. C **7**, 5084 (2019).
[54]N. Lu, H. Y. Guo, L. Li, J. Dai, L. Wang, W. N. Mei, X. J. Wu, and X. C. Zeng, "Mos_2/MX_2 heterobilayers: Bandgap engineering via tensile strain or external electrical field," Nanoscale **6**, 2879 (2014).
[55]R. Cheng, L. Yin, Y. Wen, B. Zhai, Y. Guo, Z. Zhang, W. Liao, W. Xiong, H. Wang, S. Yuan, J. Jiang, C. Liu, and J. He, "Ferromagnetism above room temperature in two intrinsic van der Waals magnets with large coercivity," Nat. Commun. **13**, 5241 (2022).
[56]W. N. Zhu, M. N. Yogeesh, S. X. Yang, S. H. Aldave, J. S. Kim, S. Sonde, L. Tao, N. S. Lu, and D. Akinwande, "Flexible black phosphorus ambipolar transistors, circuits and AM demodulator," Nano Lett. **15**, 1883 (2015).
[57]S. Bertolazzi, J. Brivio, and A. Kis, "Stretching and breaking of ultrathin MoS_2," ACS Nano **5**, 9703 (2011).
[58]A. Dewaele, P. Loubeyre, F. Occelli, O. Marie, and M. Mezouar, "Toroidal diamond anvil cell for detailed measurements under extreme static pressures," Nat. Commun. **9**, 2913 (2018).
[59]Z. Guan and S. Ni, "Strain-controllable high Curie temperature, large valley polarization, and magnetic crystal anisotropy in a 2D ferromagnetic Janus VSeTe monolayer," ACS Appl. Mater. Interfaces **12**, 53067 (2020).
[60]M. Gurram, S. Omar, and B. J. van Wees, "Bias induced up to 100% spin-injection and detection polarizations in ferromagnet/bilayer-hBN/graphene/hBN heterostructures," Nat. Commun. **8**, 248 (2017).
[61]Z. Guan, C. Si, S. Hu, and W. Duan, "First-principles study of line-defect-embedded zigzag graphene nanoribbons: Electronic and magnetic properties," Phys. Chem. Chem. Phys. **18**, 12350 (2016).
[62]S. Mangin, D. Ravelosona, J. A. Katine, M. J. Carey, B. D. Terris, and E. E. Fullerton, "Current-induced magnetization reversal in nanopillars with perpendicular anisotropy," Nat. Mater. **5**, 210 (2006).
[63]H. Meng and J. P. Wang, "Spin transfer in nanomagnetic devices with perpendicular anisotropy," Appl. Phys. Lett. **88**, 172506 (2006).
[64]B. Wang, Y. H. Bai, C. Z. Wang, S. Y. Liu, S. C. Yao, Y. Jia, and J. Cho, "Ferroelectric control of magnetic anisotropy in multiferroic heterostructure $EuSn_2As_2/In_2Se_3$," Phys. Rev. B **110**, 2469 (2024).
[65]W. R. Liu, X. J. Dong, Y. Z. Lv, W. X. Ji, Q. Cao, P. J. Wang, F. Li, and C. W. Zhang, "Magnetic anisotropy and ferroelectric-driven magnetic phase transition in monolayer $Cr_2Ge_2Te_6$," Nanoscale **14**, 3632 (2022).